J. Materials, Conc. Struct. Pavements, JSCE, No. 697/V-54, 201-214, 2002 February

MARINE DURABILITY OF 15-YEAR OLD UNCRACKED AND PRECRACKED CONCRETE MADE WITH DIFFERENT CEMENTS

Tarek Uddin MOHAMMED [1], Toru YAMAJI [2], Toshiyuki AOYAMA [3] and Hidenori HAMADA [4]

[1] Member of JSCE, JCI, JSPE, ACI and IEB (Bangladesh), Engineering Intern (Oregon State, USA), Dr. Eng., Research Engineer, Materials Division, Port and Airport Research Institute, Independent Administrative Institution (3-1-1 Nagase, Yokosuka shi, Japan 239-0826)

[2] Member of JSCE and JCI, Research Engineer, Materials Division, Port and Airport Research Institute, Independent Administrative Institution (3-1-1 Nagase, Yokosuka shi, Japan 239-0826).

[3] Member of JSCE and JCI, Civil Engineer, PS Corporation (HIB Otsuka BLDG, 3F, 1-13-17 Kita Otsuka, Toshima ku, Tokyo, Japan 170-0004)

[4] Member of JSCE, JCI, Dr. Eng., Chief Research Engineer, Materials Division, Port and Airport Research Institute, Independent Administrative Institution (3-1-1 Nagase, Yokosuka shi, Japan 239-0826)

Marine durability of 15-year old uncracked and precracked concrete specimens made with ordinary portland (OPC), slag (Type A (SCA), B (SCB) and C (SCC)) and fly ash (Type B (FACB)) cements was investigated. Compressive strength, chloride ingress, corrosion of steel bars in concrete, and crack healing were evaluated. Chloride ingress and corrosion of steel bars in concrete are sequenced as OPC>FACB>SCA>SCB>SCC. Crack healing is observed for small crack widths ($\leqq$0.5 mm) irrespective of the cement types. Large crack widths, such as 1.5, 2 and 5 mm are not healed and significant loss of diameter is observed. Voids at the steel-concrete interface cause the formation of corrosion pits.

Key Words : *fly ash cement, marine durability, ordinary portland cement and slag cement.*

1. INTRODUCTION

Utilization of blended cements in concrete is realized as it creates more durable concrete; reduces the disposal problem of the by-product of steel making industries and thermal power plants; and also indirectly the reduction of carbon dioxide emission to the atmosphere. Numerous studies have been carried out to verify the performance of concrete made with blended cements [1)~5)]. However, studies on the long-term performance of concrete made with blended cements are still necessary and will be useful to make it acceptable worldwide.

With the above-mentioned background, 15 years old tidal uncracked (cylinder specimen of diameter 15 cm and height 30 cm) and precracked (prism specimens 10×10×60 cm) concrete specimens made with ordinary portaland cement (OPC), slag cements of Type A, B and C (SCA, SCB and SCC) and fly ash cement of Type B (FACB) were investigated. These cements are specified in Japan (JIS R5211-1992 and JIS R5213-1992). Compressive strength of concrete, ultrasonic pulse velocity in concrete, water and acid soluble chloride-ion concentrations in concrete, electrochemical and physical evaluation of corrosion of steel bars in concrete and crack healing were investigated. The results are compared with the variation of cement types, such as OPC, SCA, SCB, SCC and FACB. Moreover, the study is also focused on the harmful effect of the presence of voids at the steel-concrete interface. The results of this study will be very useful in order to judge the marine durability of concrete made with different cements.

2. SCOPE AND FLOW OF INVESTIGATIONS

Uncracked cylinder specimens of diameter 15 cm and height 30 cm and precracked prism specimens of size 10×10×60 cm were investigated. The specimens

were made with ordinary portland cement (OPC), slag cement of Type A, B and C (SCA, SCB and SCC) and fly ash cement of Type B (FACB). Water-to-cement ratio was 0.45. Using these variables, reinforced concrete specimens of five cases were investigated. The specimens were exposed in a tidal pool after 28 days of standard curing and continued till this investigation, i.e., the age of 15 years. The flow of investigations is shown in **Fig.1**. Cracked and uncracked specimens are investigated in parallel.

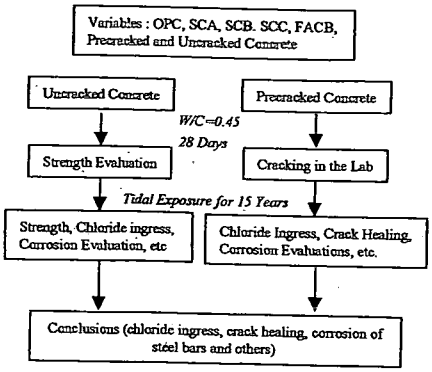

Fig.1 Flow of Investigations

3. EXPERIMENTAL PROCEDURE

(1) Materials

Ordinary portland cement (OPC), slag cement of Type A, B and C (SCA, SCB and SCC) and fly ash cement of Type B (FACB) were used. These cements are specified in Reference 6). The definitions of the blended cements and specified physical and chemical compositions can be obtained from JIS R5211-1992 and JIS R5213-1992. The compositions of the cements are listed in **Table 1.** Crushed river gravels and sand were used as coarse and fine aggregates, respectively. Specific gravity, absorption and fineness modulus of coarse and fine aggregates are listed in **Table 2.** Japanese Industrial Standard (JIS) steel bar (JIS SR 24) of diameter 9 mm was used. The yield strength of the steel bars was 230 MPa. The chemical compositions of the steel bars are listed in **Table 3.**

Table 1 Physical and Chemical Compositions of Cements

	OPC	SCA	SCB	SCC	FACB
Specific Gravity	3.16	3.07	3..03	2.97	2.97
Blaine Fineness, cm^2/g	3190	3610	3700	3980	3190
Ignition Loss (%)	0.7	0.9	0.7	0.9	0.6
SiO_2 (%)	21.3	24.9	26.5	28.9	20.4
Al_2O_3 (%)	5.3	7.8	9.2	11.3	4.7
CaO (%)	64.4	56.8	53.4	47.9	54.2
MgO (%)	2.2	3.8	4.3	5.2	1.3
SO_3 (%)	1.9	2	2	2	1.9
Na_2O (%)	0.28	-	-	-	0.45
K_2O (%)	0.6	-	-	-	0.51
TiO_2 (%)	0.37	-	-	-	-
MnO (%)	0.1	-	-	-	-
Fe_2O_3 (%)	2.6	2	1.8	1.1	2.9
P_2O_3 (%)	0.3	-	-	-	-
C (%)	0.01	-	-	-	-
S (%)	0	-	-	-	-

- not available

Table 2 Aggregate Properties

	Specific Gravity	Absorption (%)	Fineness Modulus
Sand	2.64	1.02	2.89
Gravel	2.76	1.10	6.66

Table 3 Chemical Composition of the Steel Bar

C (%)	Si (%)	Mn (%)	P (%)	S (%)
0.1	0.21	0.66	0.02	0.02

(2) Mixture Proportions

Mixture proportions of concrete are listed in **Table 4.** Water-to-cement ratio was 0.45. The slump of the fresh concrete was fixed at 8±1 cm and air content at 4±1 %. Both air-entraining and air-entraining water-reducing agents were used based on the cement weight. Mixing water was tap water.

(3) Specimens and Exposure Conditions

The plan of the specimens is shown in **Table 5.** Layout of the uncracked specimens is shown in **Fig.2.** Plain and reinforced cylindrical specimens of diameter 15 cm and length 30 cm were fabricated. In each reinforced specimen, three round steel bars of diameter 9 mm and length 18 cm were embedded at cover depths of 2, 4 and 7 cm. After standard curing, plain concrete specimens were tested for the evaluation of compressive strength at 28 days. The remaining specimens were exposed in the tidal pool till the age of 15 years. The variation of the water level and the location of the specimens in the tidal pool are shown in **Fig.3.** The specimens were located at about 0.6 m below the high water level. The average height from the high water level to the mid height of the specimens was 0.45 m. The air-drying and submerged hours were about 7 and 5 hours, respectively. Seawater was automatically pumped into the pool directly from the sea and drained out to the sea from the pool at a regular interval. The pool was located at latitude about 35° N and longitude about 138° E. The pool was free from freezing and thawing effect. The physical properties and chemical compositions of seawater are listed in **Table 6.**

Table 4 Mixture Proportions of Concrete

	OPC	SCA	SCB	SCC	FACB
G_{max} (mm)	20	20	20	20	20
Slump (cm)	8±1	8±1	8±1	8±1	8±1
Air (%)	4±1	4±1	4±1	4±1	4±1
W/C (%)	45	45	45	45	45
s/a (%)	41	42	41	41	41
W (kg/m^3)	162	160	160	162	160
C (kg/m^3)	360	356	355	360	356
S (kg/m^3)	738	756	736	714	733
G (kg/m^3)	1110	1091	1108	1120	1103
AEWRA (kg/m^3)	3.60	3.56	3.55	3.60	3.56
AEA (mL/m^3)	360	356	355	360	356

W, C, G, S (or s), and a mean water, cement, gravel, sand and aggregate (coarse and fine) respectively. AEA and AEWRA mean air-entraining, and air-entraining water-reducing admixtures respectively.

Table 5 Plan of the Specimens

Case	Uncracked Specimen (Cylinder)		Precracked Specimen (Prism)
	Plain	Reinforced*	
OPC	6+3	2	3
SCA	6+3	2	3
SCB	6+3	2	3
SCC	6+3	2	3
FACB	6+3	2	3

Six plain concrete specimens were tested at the 28-day to determine compressive strength of concrete. *One specimen of each case is retained for detail (porosity, SEM, XRD and EPMA) analysis.

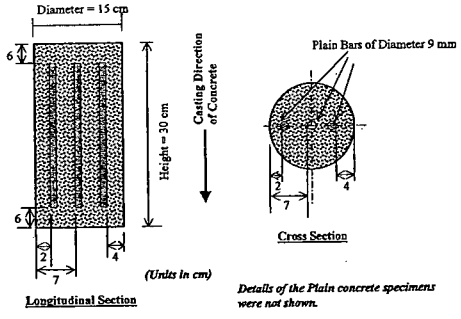

Fig.2 Details of Uncracked Cylinder Specimens

The layout of the precracked prism specimens is shown in **Fig.4.** The size of the specimens was 10×10×60 cm. In each specimen, a round steel bar of diameter 9 mm and length 50 cm was embedded at a cover depth of 4.55 cm, i.e., at the center of the specimens. After 28 days of standard curing, the

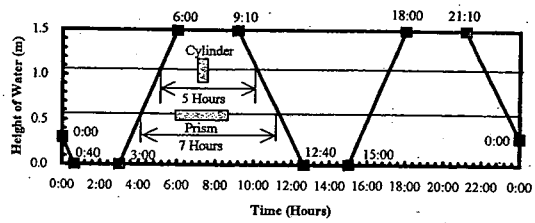

Fig.3 Variation of Water Level in the Tidal Pool and the Locations of the Cylinder and Prism Specimens

Table 6 Physical Properties and Chemical Compositions of Seawater

Sp. gr.	pH	Na ppm	K ppm	Ca Ppm	Mg ppm	Cl ppm	SO_4 ppm	CO_3 ppm
1.02	7.77	9290	346	356	1167	17087	2378	110

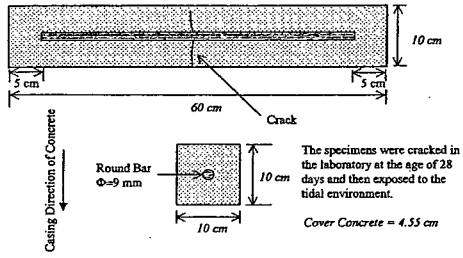

Fig.4 Details of Precracked Prism Specimens

Table 7 Applied Load and Crack Widths at the Tensile Face of the Prism Specimens

Specimen	Applied Load (in ton) and Crack Widths (mm) on the Tensile Face*		
	1	2	3
OPC	0.6 (0.2)	0.7 (0.1)	0.79 (0.1)
SCA	0.62 (0.1)	0.7 (0.3)	0.62 (0.25)
SCB	0.64 (0.5)	0.62 (0.2)	0.6 (4.0)
SCC	0.6 (1.9)	0.49 (0.15)	0.6 (2.7)
FACB	0.7 (0.1)	0.62 (0.2)	0.58 (1.5)

*The figures in the bracket indicate crack widths in mm. 1,2, and 3 are the specimen's number of each case.

specimens were cracked in the laboratory. The cracking load and the crack width on the tensile surface are listed in **Table 7.** After cracking, the specimens were exposed in the tidal pool at 0.9 m below the high water level. Air-drying and submerged hours for these specimens were about 5 and 7 hours, respectively. Further explanations on the tidal pool are already noted before.

(4) Measurements and Evaluations

a) Before Exposure

28-day compressive strength of concrete was measured as per JIS A1108. In each case, six specimens were tested. Prism specimens were cracked by bending after 28 days of standard curing. Crack widths on the tensile surface of the specimens and the applied load are already noted in **Table 7.**

b) After 15 Years of Exposure

The specimens were transferred from the exposure sites to the laboratory and cleaned with seawater. The laboratory was furnished with fresh seawater supply directly from the sea.

Compressive strength of plain concrete specimens was measured according to JIS A1108 after keeping the specimens 24 hours under seawater in the laboratory. Ultrasonic pulse velocity through the center of the plain cylinder specimens was also measured (frequency of the pulse was set at 54 kHz) before conducting compressive strength tests.

Electric wires were not connected with the steel bars embedded in concrete. To carry out electrochemical investigations, a length of 8 cm was cut from the top of the cylinder specimens. Electric wires were connected with the steel bars embedded at the different cover depths. The connection between wires and steel bars and the surrounding areas were covered with epoxy resin. Half-cell potential was measured by a Ag/AgCl half-cell. Based on the half-cell potential, the possibilities of corrosion were evaluated as per ASTM C 876 [7]. Polarization resistance and concrete resistance were measured by AC impedence technique. For this, the low frequency was set at 0.2 Hz and maximum frequency at 10 Hz. Measurements were carried out keeping the specimens submerged in seawater with a stainless steel counter electrode around the specimens. Micro-cell corrosion current was estimated based on the polarization resistance data. The extents of corrosion were evaluated as negligible, low, moderate and high for estimated current density of <0.1, 0.1-0.5, 0.5-1 and >1 $\mu A/cm^2$ respectively [8]. After these measurements, the anodic polarization curves of the steel bars embedded in the cylinder specimens were also measured. For this, the potential of the steel bars was shifted from its natural potential to a positive value of 1 V with a scan speed of 1 mV/sec by a potentiostat. The passivity grades of the steel bars were evaluated (as 0,1,2,3,4 and 5) from the measured anodic polarization curves [9]. The higher degree of passivity means the less corrosion activity. Same as cylinder specimens, a length of 6 cm was cut from one end of the prism specimens to connect electric wires with the steel bar embedded in concrete. Polarization resistance, concrete resistance and half cell potential over the steel bar of the prism specimens at the cracked region were measured with the same portable corrosion monitor. In this case, the measurements were carried out after keeping the specimens submerged in seawater for 24 hours. The corrosion sensor was furnished with a counter electrode, a guard electrode and a Ag/AgCl half cell. After electrochemical measurements, the specimens were broken open and the steel bars were collected. Corroded areas were measured. After measuring corroded area, steel bars were immersed in a 10% diammonium hydrogen citrate solution for 24 hours and then cleaned by a steel wire brush. Pit diameters were measured by an optical microscope and depth using a needle marked with known depths. The depths of the pit less than 0.5 mm were not counted.

Carbonation depth of the specimens was evaluated after spraying 1% phenolphthalein solution on freshly cut surfaces.

Water and acid soluble chloride-ion concentrations of cylinder specimens were measured at depths of 0.5-1.5, 1.5-2.5, 3.5-4.5 and 6.5-7.5 cm. For this, a disc of thickness 8 cm was cut from the middle of the reinforced concrete specimens. After cutting, the steel-concrete interfaces were checked with an optical microscope. A strip of 2-cm was again cut from the middle of the 8-cm-thick-concrete-disc and finally concrete samples were taken according to the depth as mentioned earlier. Before milling of the samples, coarse aggregates were removed carefully. Water and acid soluble chloride-ion concentrations were measured as per JCI SC4. In the case of prism specimens, only the water soluble chloride-ion concentrations were measured over the steel bars (< 5 mm from the steel bar) at cracked and uncracked regions. To measure the chloride-ion concentration at the cracked region, a strip of 5 cm was cut across the specimen keeping the crack in the middle of the strip. Then the strip was again cut to remove the portion of concrete 5 mm from the steel bar. Finally, concrete samples surrounding the steel bars were collected and water soluble chloride-ion concentration in concrete was measured as before. Same as cracked region, chloride-ion concentration at the uncracked region (10-15 cm from an end of the specimen) was also measured. Based on the water soluble chloride ion concentration, the possibilities of corrosion were evaluated as negligible, possible, probable and certain as listed in **Table 8** [10].

During the investigation, it was found that the small crack widths were healed. Therefore, possible chemical compositions of the deposit in the crack

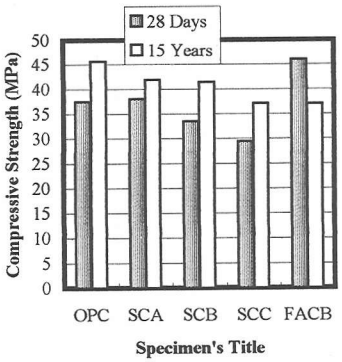

Fig.5 Compressive Strength of Concrete (at 28-day and 15-years)

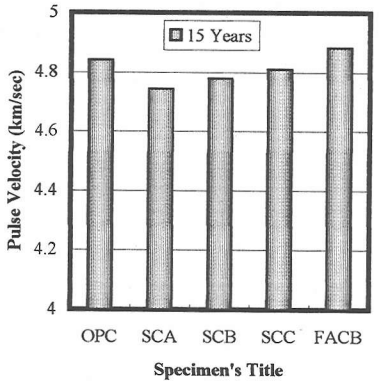

Fig.6 Pulse Velocity through Concrete (at 15-year)

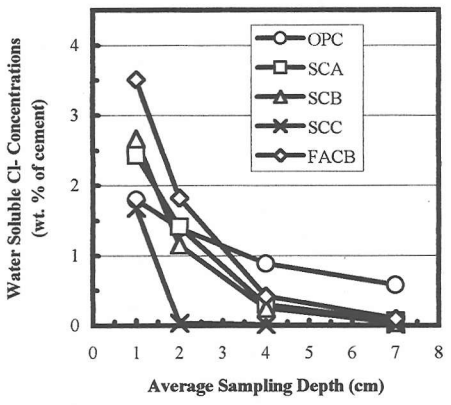

Fig.7 Water Soluble Chloride-ion Concentrations (Un-cracked Concrete)

Table 8 Chloride Threshold Values [10)]

Chloride-ion Concentration (wt. % of cement)	Possibility of Corrosion
< 0.4	Negligible
0.4 - 1.0	Possible
1.0 - 2.0	Probable
> 2.0	Certain

Table 9 Possibilities of Corrosion of Steel Bars

Cover (cm)	Possibilities of Corrosion (Based on **Table 8**)				
	OPC	SCA	SCB	SCC	FACB
2	Probable	Probable	Probable	Negligible	Probable
4	Possible	Negligible	Negligible	Negligible	Possible
7	Possible	Negligible	Negligible	Negligible	Negligible

were confirmed by EPMA (Electron Probe Micro Analyzer). Moreover, surface morphology of the deposit was also checked by SEM (Scanning Electron Microscope).

4. EXPERIMENTAL RESULTS AND DISCUSSION

(1) Carbonation Depth

The carbonation depths of the specimens were negligible irrespective of the cement types. Therefore, it could not be compared for the cements investigated here. It is understood that the specimens were subjected to chloride-ion induced corrosion only.

(2) Compressive Strength and Pulse Velocity

Compressive strengths of concrete at the age of 28 days and 15 years of exposure are shown in **Fig. 5.** Compared to the strength of 28-day, a gain in strength was observed for OPC, SCA, SCB and SCC. After 28-day, the continued hydration of concrete made with SCA, SCB and SCC and FACB will lead to increase its strength further compared to OPC. However, this gain could not be evaluated in this study as only the 28 day's and 15 year's strengths were measured. But, it was clear that after 15-year of exposure the strength of concrete made with OPC, SCA, SCB and SCC satisfied the initial design strength. Compared to the strength of 28-day, a reduction (about 20%) in strength is observed in the case of concrete made with FACB. This strength reduction is expected due to the more ettringite formation in the case of FACB. Further detail investigation on microstructure and mineralogy of the specimens is planned for the confirmation of this

result. The strength development of concrete with the continued exposure was also reported in References11)~13). A study on OPC and SCB showed that the concrete strength increased till the age of 5 years and after that reduced gradually and at the age of 20 years of exposure became the same or lower than the strength of 28 days. This strength reduction was explained due to the ettringite formation based on the mineralogical analysis of the specimens [11].

Ultrasonic pulse velocity data through the center of the concrete specimens made with different cements are shown in **Fig.6.** The pulse velocity varied in between 4.74~4.88 km/sec. No significant variation in pulse velocity was observed for the cases investigated here. The initial pulse velocity in concrete specimens was not measured. Therefore, the change in pulse velocity data as the compressive strength data could not be explained here.

(3) Chloride-ion Ingress in Concrete

a) Uncraked Concrete (Cylinder Specimens)

Water soluble chloride-ion profiles in concrete are shown in **Fig.7.** Relatively more chloride-ions were penetrated at higher depth in concrete made with OPC compared to SCA, SCB, SCC and FACB. In the case of slag and fly ash cements, accumulation of more chloride-ions was observed at the surface region, however it quickly reduced to a negligible value. The same results were also observed in another study on 10 years old concrete specimens [14]. Possibilities of corrosion of steel bars were evaluated based on the chloride-ion concentrations as mentioned in **Table 8.** The evaluated results are listed in **Table 9.** In the case of SCC, the possibilities of corrosion were negligible irrespective of the cover depths. Based on these results, chloride ingress in uncracked concrete is sequenced as OPC>FACB>SCA>SCB>SCC.

An attempt was made to determine the diffusion coefficients of chloride-ion in concrete. Fick's Second Law of diffusion is commonly used to predict the diffusion of chloride-ions in concrete. Its closed form solution is expressed as below in the literatures [15].

$$C(x,t) = C_o\left(1 - erf\left[\frac{x}{2\sqrt{D_{ac}t}}\right]\right)$$

Where, $C(x,t)$ is the chloride-ion concentration at a depth x (mm) and time t (year), C_o is the chloride-ion concentration at the surface as weight percentage of cement and D_{ac} is the apparent

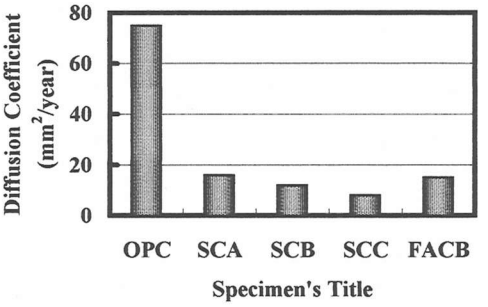

Fig.8 Diffusion Coefficient of Chloride-ion in Concrete

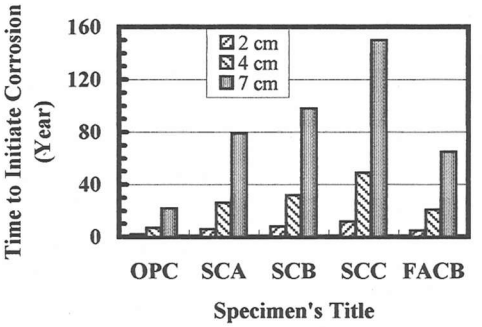

Fig.9 Time to Initiate Corrosion for Different Cements

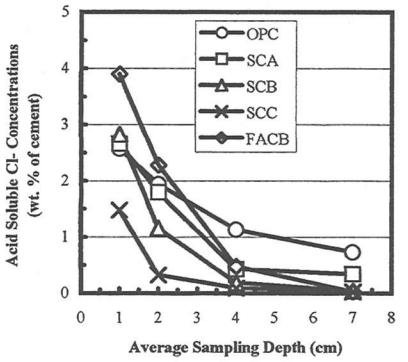

Fig.10 Acid Soluble Chloride-ion Concentrations

Table 10 Ratio of Acid to Water Soluble Chloride-ion Concentrations

*Depth (cm)	Ratio of Acid to Water Soluble Cl⁻ Concen.				
	OPC	SCA	SCB	SCC	FACB
1	1.427	1.093	1.061	0.882	1.108
2	1.392	1.264	1.006	8.013	1.249
4	1.278	1.433	0.769	6.711	1.125
7	1.262	5.456	1.183	2.797	0.313

*Depth means the average sampling depth.

Table 11 Water Soluble Chloride-ion Concentrations at the Cracked and Uncracked Regions of Prism Specimens

Specimen	Crack Widths (mm) and Water Soluble Chloride-ion Concentrations (wt. % of C) *		
	1	2	3
OPC	0.2 (1.28) ((1.27))	0.1 (1.14) ((0.64))	0.1 (1.38) ((1.41))
SCA	0.1 (0.33) ((0.17))	0.3 (0.78) ((0.23))	0.2 (0.49) ((0.43))
SCB	0.3 (0.45) ((0.31))	0.1 (0.41) ((0.28))	*5* *(3.2)* *((0.16))*
SCC	*1.5* *(1.67)* *((0.19))*	0.1 (0.37) ((0.23))	*2* *(1.84)* *((0.69))*
FACB	0.1 (0.9) ((0.67))	0.3 (0.82) ((0.29))	0.5 (1.42) ((0.27))

*The figures in (.) and ((.)) indicate chloride-ion concentration at cracked and uncracked regions respectively. The figures without bracket indicate crack widths. Unhealed cracks are noted as bold-italic letters.

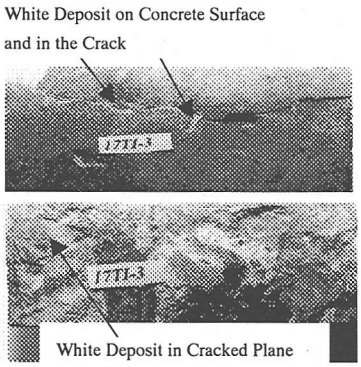

Photographs of concrete surface (top) and cracked plane (bottom) after splitting along the crack.

Fig.11 Crack Healing – FACB (Crack Width = 0.5 mm)

diffusion coefficient in mm^2/year. Here, C_o was assumed to be equal to the chloride-ion concentration at a mean sampling depth of 1 cm. The estimated average diffusion coefficient data for different cements are shown in **Fig.8.** Based on these results, chloride diffusion in concrete is also sequenced as OPC>FACB>SCA>SCB>SCC.

The time to initiate corrosion was defined as the time necessary to reach chloride-ion concentration of 0.4% of cement by weight over the steel bars. The estimated times to initiate corrosion are shown in **Fig.9** for design cover depths of 2, 4 and 7 cm. It was clearly observed that slag cement, especially SCC was very effective to increase the time to initiate corrosion. If a concrete is made with SCC and the design concrete cover is 7 cm, the theoretical time to initiate corrosion of steel bars in concrete is expected to be about 150 years.

Acid soluble chloride-ion profiles in concrete are shown in **Fig.10** for different kinds of cement investigated here. From these results, the chloride ingress into concrete is also sequenced as OPC>FACB>SCA>SCB>SCC.

The ratio of acid to water soluble chloride-ion concentrations are calculated based on the data presented in **Figs.7 and 10** and listed in **Table 10** to judge chloride binding ability of the cements. The ratio was higher for OPC compared to the other cements. It indicated that chloride binding ability of concrete made with OPC was the highest compared to the concrete made with fly ash and slag cements. It is supposed due to the superior chloride complexibility resulting in the formation of an insoluble calcium chloroalluminate compound that helps to reduce the amount of free chloride [16) ~ 18)]. There are some contradictory data in **Table 10**, especially at higher depth due to the very low chloride-ion concentrations.

b) Cracked Concrete (Prism Specimens)

Crack widths and water soluble chloride-ion concentrations of prism specimens at the cracked and uncracked regions are listed in **Table 11.** Here, crack widths measured after 15 years of exposure are noted. Relatively less chloride-ion concentration was observed at the uncracked region. In the case of large crack widths significant amount of chloride-ion concentration was observed at the cracked region. It is expected due to the accumulation of chloride-ions near the cracked region same as the accumulation of chloride-ions at the surface region (**Fig.7**). For small crack widths, slag cements showed the best performance against the chloride ingress in concrete. Chloride ingress for small crack widths ($\leqq$0.5 mm) is sequenced as OPC>FACB>SCA>SCB>SCC same as the uncracked concrete. However, the same sequence could not be concluded for large (unhealed) crack widths, such as 1.5, 2 and 5 mm.

(4) Crack Healing (Prism Specimens)

Small crack widths ($\leqq$0.5 mm) were healed by autogeneous healing irrespective of the types of cement. **Figure 11** shows a case of crack healing. White deposit was observed at the crack plane. Deposit was also extended on the surface of concrete. A detail study on the process of autogenous healing in the laboratory concluded that

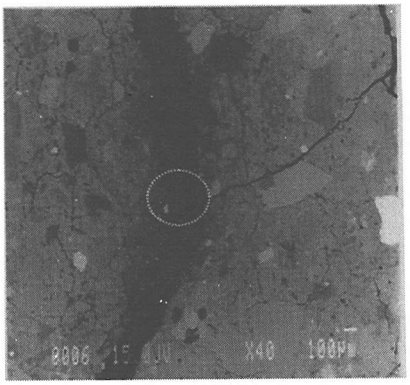

— 100 μm

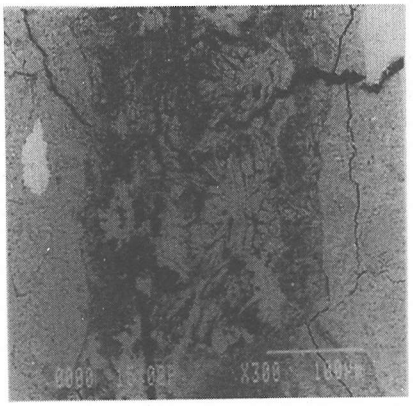

100 μm

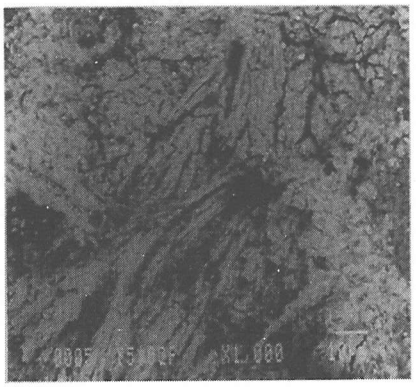

— 10 μm

Fig.12 SEM Micrographs of Concrete Surface Cutting Across the Crack (SCB)

Table 12 Half-Cell Potential (vs Ag/AgCl)

Cover (cm)	Half-Cell Potential (mV)				
	OPC	SCA	SCB	SCC	FACB
2	-274	-367	-229	-413	-338
4	-229	-182	-182	-189	-120
7	-154	-176	-169	--189	-186

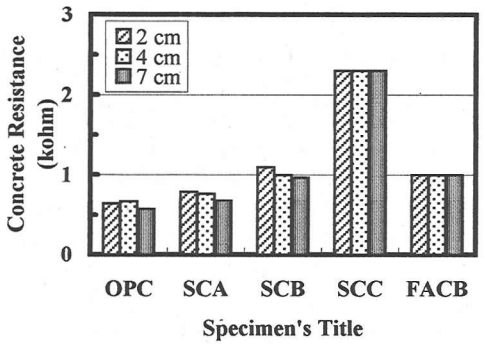

Fig.13 Concrete Resistance Over the Different Cover Depths

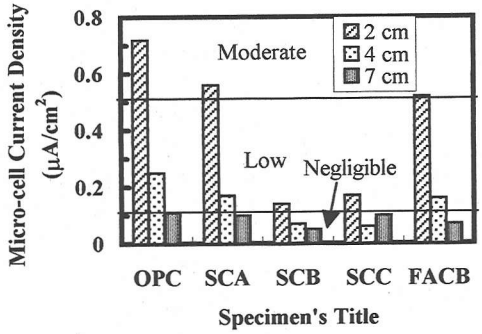

Fig.14 Micro-cell Current Density at the Different Cover Depths

the precipitation of calcium carbonate crystals ($CaCO_3$) in the cracks was almost the sole cause for the autogenous healing of the cracks [19]. The water insoluble $CaCO_3$ is evolved from a reaction between the calcium ions derived from the concrete and the in-water available bicarbonates or carbonates as shown below [19]:

$$Ca^{++} + CO_3^{--} \Leftrightarrow CaCO_3 \quad (\text{pH of water} > 8)$$

$$Ca^{++} + HCO_3^{-} \Leftrightarrow CaCO_3 + H^{+} \quad (7.5 < \text{pH of water} < 8)$$

The pH of seawater was around 7.8 **(Table 6).** Presence of alkalis in the crack regions leached from concrete and also alkali produced from the reaction of sea salts and hydrated cement pastes will increase the pH in the crack further. Therefore, the above-mentioned reactions are anticipated for the specimens investigated here.

The results of EPMA analysis indicated the presence of SO_3 with CaO and Al_2O_3 in the healed crack. From these, the presence of ettringite ($3CaO.Al_2O_3.3CaSO_4.32H_2O$) in the crack was

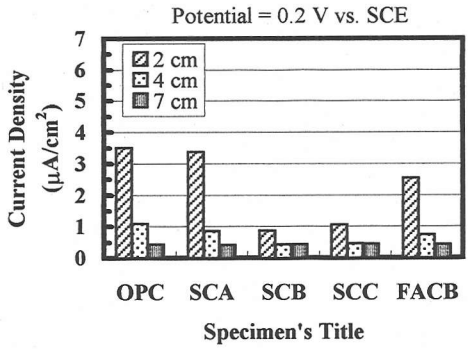

Fig.15 Current Density at Anodic Potential 0.2 V vs. SCE

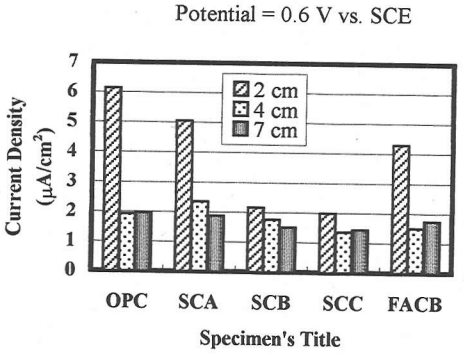

Fig.16 Current Density at Anodic Potential 0.6 V vs. SCE

Table 13 Passivity Grades of the Steel Bars

Cover (cm)	Passivity Grades				
	OPC	SCA	SCB	SCC	FACB
2	3	3	4	3	3
4	3	4	4	4	3
7	4	4	4	4	4

Table 14 Corroded Area of the Steel Bars at the Different Cover Depths – Cylinder Specimens

Cover (cm)	Corroded Area (cm^2)*				
	OPC	SCA	SCB	SCC	FACB
2	11.82	10.35	0.51	0	24.89
4	1.37	0	0	0	0
7	0	0	0	0	0

*Total Area of the Bar = 51 cm^2.

understood. EPMA results were also indicated the presence of brucite ($Mg(OH)_2$) in the healed crack. It is expected due to the reaction of magnesium salts in seawater with hydration products of cement. SEM micrographs across the cracked region are shown in **Fig.12**. The needle-shaped ettringite was mixed with other deposits, such as calcite ($CaCO_3$) and brucite.

The progress of healing with the variation of the cement types could not be judged from this investigation. However, in Reference19) based on a detail laboratory study, it was concluded that the type of cements has no influence on the autogenous healing [19]. Therefore, for the same crack widths, the progress of healing can be assumed to be the same irrespective of the cement types, such as OPC, SCA, SCB, SCC and FACB. Healed crack widths ($\leqq$0.5 mm) are defined here as small crack widths. Unhealed crack widths, such as 1.5 mm, 2 mm and 5 mm are defined as large crack widths.

(5) Corrosion of Steel Bars in Concrete: Electrochemical Evaluations

a) Uncracked Concrete (Cylinder Specimens)

Half cell potential data over the steel bars embedded in cylinder specimens are presented in **Table 12.** For a deeper cover depth, a tendency of lower negative potential was observed. For SCC, the steel bar located at a depth of 2 cm cover depth showed relatively more negative potential, however corroded area over the steel bars was lower compared to the others (corroded area is explained later). In another study, it was also found that steel bars located at very high negative potentials were not corroded at all even though the active corrosion potential was evaluated based on Reference12). Therefore, based on the half cell potential data, degree of corrosion of the steel bars is not sequenced here.

Concrete resistance data over the steel bars located at the different cover depths are shown in **Fig.13**. Generally, ion movement in low resistance concrete is higher than the relatively high resistance concrete. It causes to increase corrosion rate in low resistance concrete. Lower concrete resistance was observed in the case of OPC compared to slag and fly ash cements. SCC showed the highest concrete resistance among the cements investigated here. Therefore, the lowest corrosion activity is expected for blended cements, especially for SCC and SCB compared to OPC. No significant difference in concrete resistance was observed for concrete over 2, 4 and 7 cm of cover depths.

Utilizing polarization resistance data, micro-cell current density of the steel bars was evaluated from the Stern-Geary equation as below [20] :

$$I_{mic} = \frac{B}{R_p} \times 10^6$$

$$B = \frac{\beta_a \beta_c}{2.3(\beta_a + \beta_c)}$$

Where, I_{mic} is the micro-cell current density in $\mu A/cm^2$, the value of constant B depends on the slopes of the anodic (β_a) and cathodic (β_c) polarization curves. Assuming, β_a and β_c as 120 mV/decade as the average of all corrosion system, the value of B can be estimated at 0.026 V [8), 20), 21)]. R_p is the polarization resistance in ohm.cm^2. Calculated micro-cell current density of the steel bars located at the different cover depths are shown in **Fig.14**. The extents of corrosion based on the micro-cell current density were also evaluated as negligible, low, moderate and high for current density of <0.1, 0.1-0.5, 0.5-1.0 and >1 $\mu A/cm^2$ respectively [8)]. Lower current density was observed for a greater cover depth. It can be explained due to the lower chloride-ion concentrations as well as the lower oxygen permeability at larger cover depths [22), 23)]. At cover depth of 2 cm, relatively more current density was observed for concrete made with OPC, FACB and SCA. It is expected due to the presence of more chloride-ions over the steel bars located at 2 cm cover depth (**Fig.7**). Also, there are other factors, such as the ratio of Cl^-/OH^- and concrete resistance that influence the corrosion rate significantly [24), 25)]. Relatively less micro-cell corrosion was observed for concrete made with slag cements, especially SCC and SCB.

From the anodic polarization curves, current densities at potentials 0.2 V and 0.6 V were evaluated and the results are shown in **Figs.15 and 16.** Relatively lower current density was observed in the case of slag cements, especially for SCC. Passivity grades of the steel bars evaluated from the anodic polarization curves are listed in **Table 13** based on the Reference9). Higher grades of passivity indicate less corrosion activity. A tendency of higher grade of passivity was observed for the steel bars located at the deeper cover depth. Also, a tendency of higher grade of passivity was observed for the steel bars in concrete with slag cements.

Based on the above-mentioned electrochemical results, the degree of corrosion of steel bars in uncracked concrete is sequenced as OPC>FACB>SCA>SCB>SCC.

b) Cracked Concrete (Prism Specimens)

Micro-cell current density of the steel bars at the cracked region of the prism specimens are shown in **Fig.17**. For small crack widths (≦0.5 mm), a tendency of having lower current density (0.1-0.5 $\mu A/cm^2$) was observed due to the healing of the cracks. It is already mentioned that the small crack widths (≦0.5 mm) were healed during the exposure

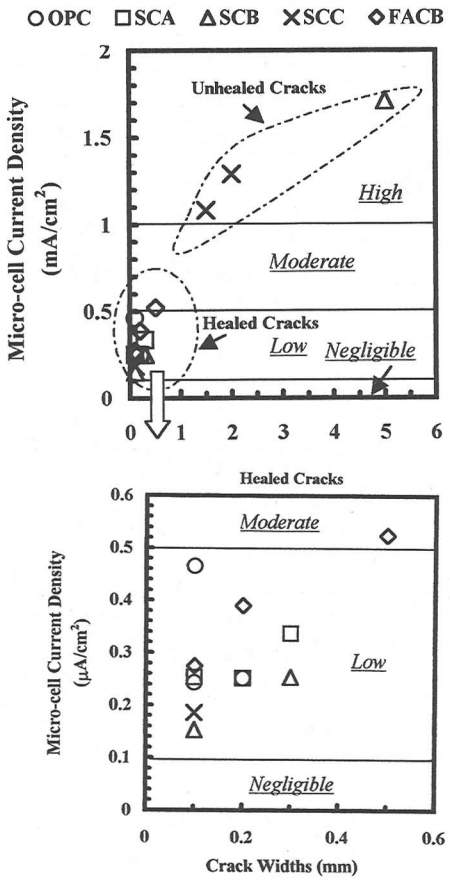

Fig.17 Micro-cell Current Density at the Cracked Regions (Top: Large and Small Crack Widths, Bottom : Small Crack Widths Only)

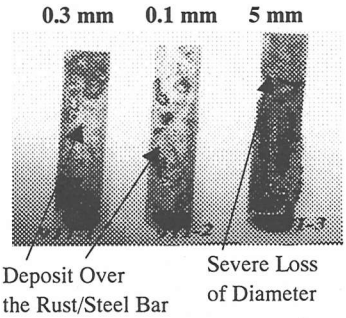

Fig.18 Steel Segments at the Cracked Region – SCB

in the tidal pool for 15 years. The healing caused to cease or reduce the corrosion rate. For the healed crack no significant relation between the crack widths (≦0.4 mm) and the corrosion rate was found, however, a tendency of having more corrosion was

observed for healed crack of size 0.5 mm compared to the small crack widths ≦0.4 mm. Same kind of observation was also observed in the physical evaluation. The deposit was also covered the rust over the steel bar near the crack as shown in **Fig.18.** Therefore, it is expected that the corrosion process is stopped or reduced significantly due to the healing as mentioned before. The degree of corrosion is sequenced as OPC>FACB>SCA>SCB>SCC for small crack widths.

Large crack widths (1.5, 2 and 5 mm) were not healed. Higher amount (>1.0 $\mu A/cm^2$) of micro-cell current density was observed at these cracks. Significant loss of diameter was observed due to the corrosion around the perimeter of the steel bar as shown in **Fig.18.** Chloride-ion induced corrosion is well known as an autocatalytic process [26]. It lowers the pH value surrounding the steel bars and accumulates positive ions (Fe^{++}) at the cracked regions. The excess positive charges are balanced by the migration of chloride-ions. It is clear that in the case of small crack widths with the progress of crack healing the autocatalytic process is stopped or reduced significantly. On the other hand, the progress of the autocatalytic reaction continues in the case of large crack widths and leaded to a significant loss of diameter due to the corrosion of steel bars around the perimeter. Very high amount of chloride-ions at the cracked region was also found at the large crack widths (**Table 11**).

(6) Corrosion of Steel Bars in Concrete: Physical Evaluations

a) Uncracked Concrete (Cylinder Specimens)

Corroded areas of the steel bars of uncracked specimens (cylinder specimens) are listed in **Table 14.** It was observed that at 2 cm of cover depth, corroded area was highest for FACB. Slag cements showed the best performance against the corrosion of steel bars. In the case of SCC, the corroded areas were mostly concentrated at the voids surrounding the steel bar.

Number of pits and maximum pit depths are listed in **Table 15.** Steel bars in concrete made with OPC and FACB showed more number of pits compared to SCA, SCB and SCC. SCC showed the least number of pits. Based on these results, degree of corrosion of steel bars in concrete is sequenced as OPC>FACB>SCA>SCB>SCC. This confirms the electrochemical results explained before.

b) Cracked Concrete (Prism Specimens)

The maximum pit depths of the steel bars at the cracked and uncracked regions of prism specimens are listed in **Table 16.** For small crack widths (≦ 0.5 mm), maximum pit depth was not necessarily

Table 15 Number of Pits and Maximum Pit Depth - Cylinder Specimens *

Cover (cm)	Number of Pits and Maximum Pit Depth (mm)				
	OPC	SCA	SCB	SCC	FACB
2	6 (1.5)	3 (1)	0 (0)	0 (0)	5 (0.5)
4	2 (1)	0 (0)	0 (0)	0 (0)	0 (0)
7	0 (0)	0 (0)	0 (0)	0 (0)	0 (0)

* Pit depths <0.5 mm were neglected. The figures in the bracket indicate maximum pit depth in mm.

Table 16 Crack Widths and Maximum Pit Depths – Prism Specimens

Specimen	Crack Widths (mm) and Maximum Pit Depths at Cracked and Uncracked Regions (mm) *		
	1	2	3
OPC	0.2 (0.5) ((1.0))	0.1 (0) ((0.5))	0.1 (0.5) ((1.5))
SCA	0.1 (0) ((0))	0.3 (0.5) ((1.0))	0.2 (0) ((0))
SCB	0.3 (0.5) ((0))	0.1 (0) ((0))	*5* *(3.5**)* *((0))*
SCC	*1.5* *(1**)* *((0))*	0.1 (0) ((0))	*2* *(0.5**)* *((0))*
FACB	0.1 (0.5) ((0.5))	0.3 (1.0) ((0.5))	0.5 (1.5) ((0.5))

*The figures in (.) and ((.)) indicate maximum pit depths at cracked and uncracked regions respectively. Pit depths < 0.5 mm were not counted. The figures without bracket indicate crack widths. Unhealed cracks are noted as bold-italic letters. **Significant loss of diameter was observed due to the corrosion of steel bars around the perimeter.

Table 17 Crack Widths and Total Number of Pits – Prism Specimens

Specimen	Crack Widths (mm) and Pit Numbers		
	1	2	3
OPC	(0.2) 7	(0.1) 5	(0.1) 8
SCA	(0.1) 0	(0.3) 7	(0.2) 7
SCB	(0.3) 2	(0.1) 0	(5) 3
SCC	(1.5) 1	(0.1) 0	(2) 1
FACB	(0.1) 4	(0.3) 4	(0.5) 4

The figures in (.) indicate crack widths in mm.

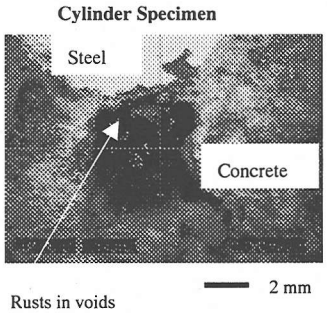

Fig.19 Steel-Concrete Interface of Cylinder Specimen - SCB

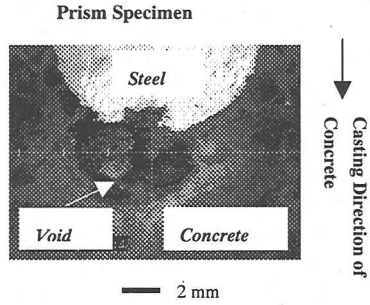

Fig.20 Pit on the Steel Bar due to the Void (Prism Specimen – OPC)

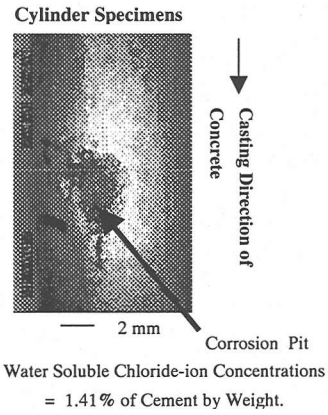

Fig.21 Pit on the Steel Bar due to the Void (Prism Specimen – SCA)

observed at the cracked regions. It is explained due to the crack healing. SCC showed the least number of pits. The total numbers of pit are listed in **Table 17**. Pit numbers in the case of slag cements, especially SCC was the lowest. For small crack widths (≦0.5 mm), the degree of corrosion of steel bars is sequenced as OPC>FACB>SCA>SCB>SCC as in uncracked concrete. This also confirms the electrochemical results explained before.

For large crack widths (1.5, 2 and 5 mm), significant loss of diameter was observed due to the corrosion of steel bar around the perimeter (**Fig. 18** and **Table 16**). Unfortunately, due to the limited number of data relevant to the large crack widths, the performance of the cements investigated here could not be compared. Further investigations are still necessary on this matter. Deep localized corrosion is suspected for blended cements based on the limited numbers of data (**Table 16**). It is understood that in order to enhance durability of concrete structures in the marine environment, crack widths should be narrower to allow possible healing during its exposure.

(7) Influence of Voids at the Steel Concrete Interface

Several detail laboratory and long-term exposure investigations on the influence of voids at the steel concrete interfaces were carried out. The results were reported in References27)~30). Here, the voids are defined as the visible voids by naked eyes. The size of the void is in the order of a mm to a few mm in diameter. The voids may also be continued under the horizontal steel bars where the casting direction is perpendicular to the steel bar and the casting height is large. It was observed that the presence of voids at the steel-concrete interface caused the formation of corrosion pits. For sound steel-concrete interface, steel bars were not corroded at all even for a chloride-ion concentration much more than the chloride threshold limit defined as 0.4% of cement by weight. Microscopic views on the formation of corrosion pits due to the voids at the steel-concrete interfaces are shown in **Figs.19 ~21**. If the casting direction of concrete is perpendicular to the steel bar (**Fig.20**, Prism specimens), voids under the steel bars form due to the settlement of concrete against the gravity as well as the trapping of bleeding water under the bar. The voids can also create over the steel bar even though the casting direction is along the steel bar (**Fig.19**, Cylinder Specimens) due to the poor compaction of concrete. During this investigation, it was observed that corroded areas in the case of slag cements were very low and just concentrated at the void at steel-concrete interface. Therefore, in order to enhance long-term durability of concrete structures in the

marine environment, steel-concrete interfaces should be free from voids

(8) Remaining Studies

Microstructures of concrete (porosity), surface morphology (SEM), chemical compositions (XRD and EPMA) of concrete made with the cements investigated here are still continuing. The results will be reported in future. Some specimens are still retained in the exposure sites and will be investigated at the 20-year of exposure.

5. CONCLUSIONS

Based on the investigations on 15 years old tidal uncracked and precracked concrete specimens made with W/C=0.45 and different kinds of cement, such as ordinary portland cement (OPC), slag cements of Type A (SCA), B (SCB) and C (SCC), and fly ash cement of Type B (FACB), the following conclusions are drawn:

1. Chloride ingress and corrosion of steel bars in concrete are sequenced as OPC>FACB>SCA>SCB>SCC for uncracked and cracked concrete with small crack widths ($\leqq$0.5 mm).

2. After 15 years of exposure in the tidal environment, compressive strengths of concrete satisfy the corresponding design strength of 28-day, except FACB.

3. Small crack widths ($\leqq$ 0.5 mm) heal irrespective of the cement types.

4. The presence of visible voids at the steel-concrete interface causes the formation of corrosion pits irrespective of the cement types.

5. In order to enhance long-term durability, crack widths should be controlled for possible healing during exposure and concrete structures should be made without voids at the steel-concrete interface.

ACKNOWLEDGEMENT: The authors wish to express their gratitude and sincere appreciation to the authority of *Port and Airport Research Institute, Independent Administrative Institution, Yokosuka, Japan* for giving support to perform this investigation. Thanks are due to the members of the *Materials Division of Port and Airport Research Institute* for their kind help during the experimental works. Thanks are also due to the previous members of the Materials Division of Port and Airport Research Institute for preparing the layout of these precious specimens before 15 years.

REFERENCES

1) Nagataki, S.: Mineral Admixtures in Concrete : State of the Art and Trends, Proceedings of V. Mohan Malhotra on Concrete Technology Past, Present and Future, *ACI SP 144*, pp. 447-482, 1993.
2) Mehta, P. K.: Pozzolanic and Cementitious By-Products as Mineral Admixtures for Concrete – A Critical Review, Proc. Of the CANMET/ACI First International Conference, *ACI SP 79*, Vol. 1, pp. 1-46, 1983.
3) Malhotra, V.M.: Fly Ash, Slag, Silica Fume, and Rice-Husk Ash in Concrete : A Review, *ACI Concrete International*, Volume 15, No. 4, pp. 23-28, 1993.
4) RILEM Report &, Fly Ash in Concrete - Properties and Performance, Editor Wesche, K., Chapman and Hall, 1991.
5) Malhotra, V.M. and Mehta, P.K.: Pozzolanic and Cementitious Materials, Advance in Concrete Technology, Vol. 1, Gordon and Breach Publishers, Canada, 1996.
6) Standard Specification for Design and Construction of Concrete Structures, Japan Society of Civil Engineers, Part 2 (Construction), SP-2, First Edition, 1986.
7) ASTM C876-91, Standard Test Methods for Half-Cell Potential of Uncoated Reinforcing Steel in Concrete, 1991.
8) Andrade, C. and Alonso, C.: On-site Measurement of Corrosion Rate of Reinforcements, Fifth CANMET/ACI International Conference on Durability of Concrete, Barcelona, Spain 2000, Proceedings of a Special Technical Session on "Near-Surface Testing for Strength and Durability of Concrete", Ed. Basheer, P.A.M., pp.171-183, 2000.
9) Otsuki, N., Nagataki, S. and Nakashita, K.: Evaluation of AgNO3 Solution Spray Method for Measurement of Chloride Penetration into Hardened Cementitious Materials, *ACI Materials Journal*, Vol. 89, No. 6, pp. 587-592, Nov.-Dec. 1992.
10) Brown, R.D.: Mechanism of Corrosion of Steel in Concrete in Relation to Design, Inspection and Repair of Offshore and Coastal Structures, Performance of Concrete in Marine Environment, *ACI SP 65*, pp. 169-204, 1980.
11) Fukute, T. and Hamada, H.: A Study on the Durability of Concrete Exposed in Marine Environment for 20 Years, *Report of the Port and Harbour Research Institute*, Ministry of Transport, Japan, Vol. 31, No. 5, pp. 251-272, March 1993.
12) Mohammed, T.U., Otsuki, N., Hisada, M. and Hamada, H.: Marine Durability of 23-Year-Old Reinforced Concrete Beams, Fifth CANMET/ACI International Conference on Durability of Concrete, Barcelona, Spain, *ACI SP 192-65*, pp.1071-1088, 2000.

13) Sakai, K.: Long-Term Performance of Concrete in a Marine Environment, Third CANMET/ACI International Conference on Performance of Concrete in Marine Environment, pp. 35-53, August 1996.
14) Sakai, K. and Sasaki, S.: Ten Year Exposure Test of Pre-Cracked Reinforced Concrete Specimens in a Marine Environment, *ACI SP145-18*, pp. 353-369, 1994.
15) Hansen, E. J. and Saouma, V.E.: Numerical Simulation of Reinforced Concrete Deterioration – Part I : Chloride Diffusion, *ACI Materials Journal*, Vol. 96, No. 2, pp. 173-180, March-April 1999.
16) Rasheeduzzafar, A.S., Dakhil, S.S. and Al-Gahtani, A.S.: Effect of Cement Composition on Corrosion of Reinforcing Steel in Concrete, Third International Symposium on Corrosion of Reinforcement in Concrete Construction, U.K., Edited by Page, C.L., pp. 213-226, 1990.
17) Mehta, P.K.: Durability of Concrete Exposed to Marine Environment – A Fresh Look, 2nd CANMET/ACI International Conference on Durability of Concrete, Canada, *ACI SP 109-1*, pp. 1-29, 1991.
18) Rosenberg, A., Grace, W.R. and Hansson, M.C.: Mechanisms of Corrosion of Steel in Concrete, *Materials Science of Concrete*, Vol. 1, Skanly Jp. Ed., MRS, pp. 285-316, 1989.
19) Edvardsen, C.: Water Permeability and Autogenous Healing of Cracks in Concrete, *ACI Materials Journal*, V. 96, No. 4, pp. 448-454, July – August 1999.
20) Fontana, M. G. and Greene, N. D.: Corrosion Engineering, Second Edition, McGraw-Hill, 1983.
21) Gu, P., Beaudoin, J.J., Zhang, M.H. and Malhotra, V.M.: Performance of Reinforcing Steel in Concrete Containing Silica Fume and Blast-Furnace Slag Ponded with Sodium Chloride Solution, *ACI Materials Journal*, Vol. 97, No. 3, pp. 254-262, May-June 2000.
22) GjØrv, O.E., Vennesland, O. and El-Busaidy, A.H.S.: Diffusion of Dissolved Oxygen Through Concrete, *Materials Performance*, 25, 12, pp. 38-44, 1986.
23) Sandberg, P.: Cost Effective Service Life Design of Concrete Structures in Saline Environment, Proceedings of the International Conference on Durability of Building Materials and Components, Vol. 2, pp. 1195-1214, 1996.
24) Mehta, P.K.: Concrete : Structure, Properties and Materials, Prentice – Hall, Englewood Cliffs, New Jersey.
25) Monterio, P.J.M., GjØrv, O.E. and Mehta, P.K.: Microstructure of the Steel-Cement Paste Interface in the Present of Chloride, *Cement and Concrete Research*, Vol. 15, pp. 781-784, 1985.
26) Gu, P., Beaudoin, J.J., Tumidajski, P.J. and Mailvaganam, N.P.: Electrochemical Incompatibility of Patches in Reinforced Concrete, *Concrete International*, Vol. 19, No. 8, pp. 68-72, August 1997.
27) Mohammed, T.U, Otsuki, N. and Hisada, M.: Corrosion of Steel Bars with Respect to Orientation in Concrete, *ACI Material Journal*, Vol. 96, No. 2, pp. 154-159, March – April 1999.
28) Mohammed, T.U., Hamada, H., Otsuki, N. and Toru, Y.: Chloride-ion Induced Corrosion of Steel Bars in Concrete with the Presence of Gap at the Steel-concrete Interface, *ACI Materials Journal* (to be published in March – April 2002 issue).
29) Mohammed, T.U., Otsuki, N., Hamada, H. and Watanabe, H.: Several Issues in Designing Durable RC Structures, Journal of JCI, Vol. 38, No. 11, pp. 36-41, November 2000 (Japanese).
30) Mohammed, T.U.: A Study on Corrosion of Plain and Deformed Steel Bars With Respect to Bar Orientation and Cracks in Concrete, Doctoral Thesis, Department of Civil Engineering, Tokyo Institute of Technology, Japan, September 1997.

(Received February 5, 2001)

ひびわれの有無およびセメント種の異なるコンクリートの海洋環境下における耐久性（暴露 15 年試験結果）

Tarek Uddin MOHAMMED・山路徹・青山敏幸・濵田秀則

普通セメント（OPC），高炉スラグセメントA種（SCA），B種（SCB），C種（SCC）およびフライアッシュセメントB種（FACB）を用い，ひびわれの有無の異なるコンクリート試験体の海洋環境下における暴露 15 年試験を実施し，圧縮強度，可溶性・全塩化物含有量，ひびわれ治癒（閉塞），および埋設鉄筋の電気化学的性状および物理的性状に関する試験を行った．塩化物の浸入量および鉄筋の腐食量をセメント種で比較すると，概ね OPC＞FACB＞SCA＞SCB＞SCC，の順になった．また，セメント種によらず，ひび割れ幅が概ね 0.5mm 以下の場合，ひびわれ治癒（閉塞）が認められたが，0.5mm よりも大きな場合，ひびわれ治癒は観察されなかった．コンクリートと鋼材の界面に空隙が存在する箇所において孔食が生じていた．